FULL PAPER

Performances of Liquid-Exfoliated Transition Metal Dichalcogenides as Hole Injection Layers in Organic Light-Emitting Diodes

Cheolmin Kim, Thang Phan Nguyen, Quyet Van Le, Jong-Myeong Jeon, Ho Won Jang, and Soo Young Kim**

2D transition metal dichalcogenide (TMD) nanosheets, including MoS_2, WS_2, and TaS_2, are used as hole injection layers (HILs) in organic light-emitting diodes (OLEDs). MoS_2, WS_2, and TaS_2 nanosheets are prepared using an exfoliation by ultrasonication method. The thicknesses and sizes of the TMD nanosheets are measured to be 3.1–4.3 nm and more than 100 nm, respectively. The work functions of the TMD nanosheets increase from 4.4–4.9 to 4.9–5.1 eV following ultraviolet/ozone (UVO) treatment. The turn-on voltages at 10 cd m^{-2} for UVO-treated TMD-based devices decrease from 7.3–12.8 to 4.3–4.4 V and maximum luminance efficiencies increase from 5.74–9.04 to 12.01–12.66 cd A^{-1}. In addition, this study confirms that the stabilities of the devices in air can be prolonged by using UVO-treated TMDs as HILs in OLEDs. These results demonstrate the great potential of liquid-exfoliated TMD nanosheets for use as HILs in OLEDs.

1. Introduction

Organic light-emitting diodes (OLEDs) have received significant attention as next-generation display and solid-state lighting materials because they are inexpensive, light weight, and flexible.[1–4] In order to reduce driving voltages and increase efficiencies, many researchers have attempted to reduce the energy barriers of electrode/organic interfaces to facilitate charge carrier injection.[5,6] Poly(3,4-ethylenedioxythiophene):poly(styrene-sulfonate) (PEDOT:PSS) is widely used both as a hole injection layer (HIL) and to reduce energy barriers owing to its suitable work function (≈5.0 eV). However, PEDOT:PSS is not suitable for practical applications because of its hygroscopicity and acidity, which cause rapid degradation of OLEDs by etching their indium tin oxide electrodes.[7,8]

Recently, 2D transition metal dichalcogenides (TMDs) have been studied[9–12] and applied in a wide range of applications, such as batteries, field-effect transistors, catalysis, and solar cells, because of their superior carrier mobilities. Their superior carrier mobilities are caused by ballistic transport, enhanced photoluminescences that result from quantum confinement effects, and larger band gaps than those observed in the bulk material.[13–16] It is believed that the presence of lone pairs of electrons at the surfaces of TMDs and the absence of dangling bonds could enhance their resistances to reactions with other chemical species. Therefore, TMD nanosheets are expected to be applied in OLEDs as HILs to improve stability. However, the work functions of TMD nanosheets are not high enough (MoS_2 = ≈4.7 eV,[17] WS_2 = ≈4.6 eV,[18] TaS_2 = ≈4.4 eV[13] for them to improve the performances of OLEDs when used as HILs. 2D TMDs can be prepared by mechanical cleavage, liquid exfoliation, and chemical vapor deposition methods.[19–28] The mechanical cleavage method is unsuitable for mass production applications because it is not scalable and does not provide control over product thickness or size. The chemical vapor deposition method still needs to be improved before it can be used to produce uniform TMDs. In contrast, exfoliation by ultrasonication is the simplest production method and can be used for large-scale production of 2D nanosheets at room temperature. Therefore, surface treatment and liquid exfoliation methods were used to implement TMD nanosheets as HILs in OLEDs in this study.

In this paper, we fabricated green OLEDs using MoS_2, WS_2, and TaS_2 nanosheets, instead of PEDOT:PSS, as HILs. MoS_2, WS_2, and TaS_2 nanosheets were obtained using an exfoliation method that makes use of an ultrasonicator as shown **Figure 1**. Exfoliated materials were spin-coated onto the indium tin oxide (ITO) glass substrates to form ultrathin nanosheets. The nanosheets were treated with ultraviolet/ozone (UVO) to modulate their work functions and improve the performances and stabilities of the OLEDs produced. Herein, we discuss the properties and performances of OLEDs produced with these TMD nanosheets.

C. Kim, T. P. Nguyen, Q. V. Le, Prof. S. Y. Kim
School of Chemical Engineering
and Materials Science
Chung-Ang University
Seoul 156-756, Republic of Korea
E-mail: sooyoungkim@cau.ac.kr
J.-M. Jeon, Prof. H. W. Jang
Department of Materials Science and Engineering
Research Institute of Advanced Materials
Seoul National University
Seoul 151-744, Republic of Korea
E-mail: hwjang@snu.ac.kr

DOI: 10.1002/adfm.201501333

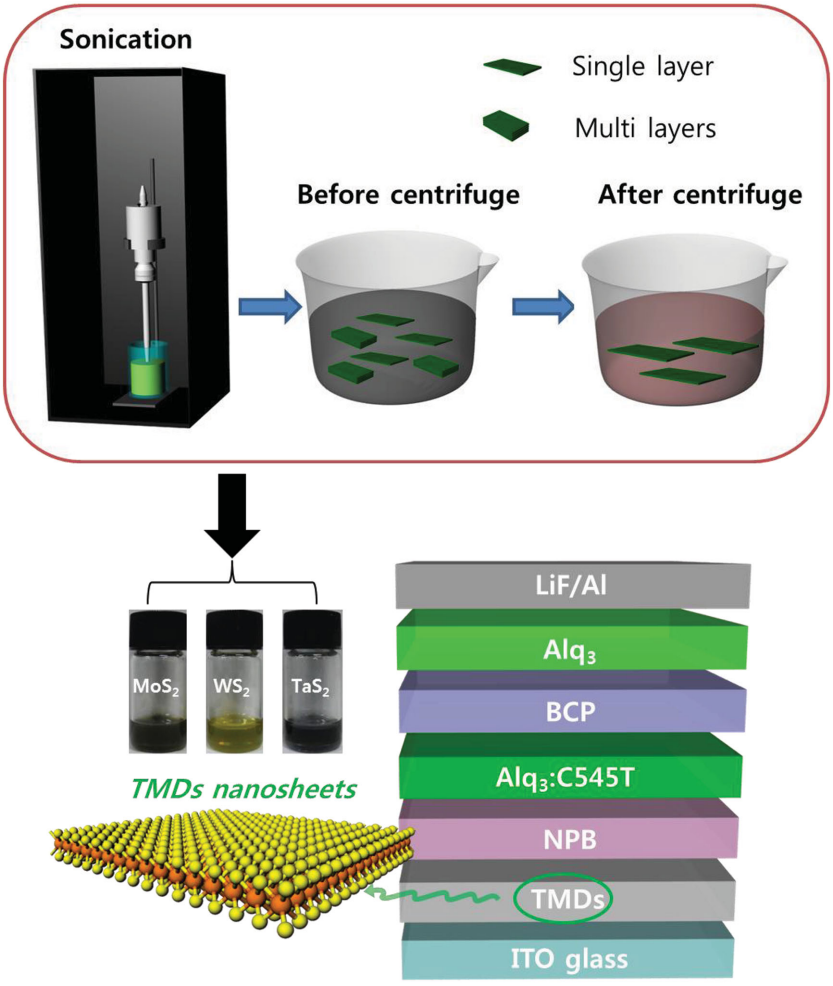

Figure 1. The structures of OLEDs. The images of MoS_2, WS_2, and TaS_2 dispersed in vial are also shown.

2. Results and Discussion

Figure 2 shows the UV–vis absorption spectra of bulk-TMDs and exfoliated-TMD nanosheets. No detectable peaks were observed in the spectra of bulk MoS_2, WS_2, and TaS_2 samples prior to ultrasonication. It is thought that bulk TMDs have indirect band gaps; therefore, absorption peaks do not appear in their UV–vis absorption spectra. The two adsorption peaks in the spectrum of exfoliated-MoS_2 (610, 671 nm) and the single peaks in the spectra of exfoliated-WS_2 (624 nm) and exfoliated-TaS_2 (472 nm) correspond to direct excitonic transitions at the K-points of Brillouin zones.[9,13,16] Optical band gaps were calculated from absorption edges using the equation, $E_g = hc/\lambda$ (E_g: energy gap; h: Planck's constant; c: the speed of light). The optical band gaps of MoS_2, WS_2, and TaS_2 nanosheets were calculated to be 1.70, 1.80, and 1.63 eV, respectively. These results indicate that the band gaps of TMD materials change from being indirect to direct as layer numbers decrease. We attribute this to quantum confinement effects.[9] To measure the thicknesses and sizes of the TMD nanosheets, the surfaces of the nanosheets were scraped and examined by atomic force microscopy (AFM). Statistical data of the layer number distribution for exfoliated TMDs are shown in Figure S1 in the Supporting Information. It is shown that the most of exfoliated TMDs have one to three layers. The scraped image is shown in Figure S2 in the Supporting Information. The thicknesses of the MoS_2, WS_2, and TaS_2 nanosheets were determined to be 4.1, 4.3, and 3.1 nm, respectively, as shown in Figure 2b–d. The substrate with 2D nanosheets displayed clean AFM images as shown in Figure S3 in the Supporting Information. Furthermore, the surface roughness is as low as 0.638, 0.735, and 0.271 nm for MoS_2, WS_2, and TaS_2, respectively. These results indicated that ITO surfaces are fully covered with TMDs nanosheets. The transmission electron microscopy (TEM) images shown in the insets of Figure 2 indicate that the TMDs nanosheets were larger than 100 nm. These results indicate that the exfoliation method used produced TMD nanosheets only a few layers thick.

X-ray diffraction (XRD) patterns of exfoliated-TMDs and bulk-TMDs are shown in **Figure 3**. The bulk materials show various peaks due to the reflection of lattice planes, indicating that bulk materials have many layers. After sonication and removal of TMDs with large size, only one peak of (002) exists with weaker intensity. The disappearance of the other peaks in XRD pattern indicates that one layer or few layers of TMDs nanosheets were successfully made through the exfoliation process.[29]

Figure 4 shows the TEM images of exfoliated a) MoS_2, b) WS_2, and c) TaS_2 nanosheets. The selected area electron diffraction (SAED) patterns shown in the insets of Figure 4 indicated that exfoliated TMD materials still have hexagonal lattice structure. The lattice constants of MoS_2, WS_2, and TaS_2 measured from TEM image are 0.32, 0.32, and 0.34 nm, respectively. Metal atoms and sulfur atoms can also be identified in TEM images. The yellow point and blue point correspond with metal atom and sulfur atom in hexagonal structure. These results indicated that exfoliated TMD materials consist of stacking layers, which is consistent with the previous report.[30]

Figure 5 shows the synchrotron radiation photoelectron spectroscopy (SRPES) spectra of the TMD nanosheets. Mo 3d peaks are located at 228.5 and 231.6 eV and correspond to the Mo^{4+} $3d_{5/2}$ and Mo^{4+} $3d_{3/2}$. W 4f peaks are located at 32.3 and 34.6 eV and correspond to W^{4+} $4f_{7/2}$ and W^{4+} $4f_{5/2}$ transitions. Following UVO treatment for 15 min, new Mo 3d peaks appeared at 232.7 and 235.6 eV in MoS_2 samples, corresponding to Mo^{6+} $3d_{5/2}$ and Mo^{6+} $3d_{3/2}$ transitions. In WS_2 samples, new W 4f peaks appeared at 35.5 and 37.7 eV, corresponding to W^{6+} $4f_{7/2}$ and W^{6+} $4f_{5/2}$ transitions. The intensity of the Mo^{6+} portion of the Mo 3d peak and that of the W^{6+} portion of the W 4f peak

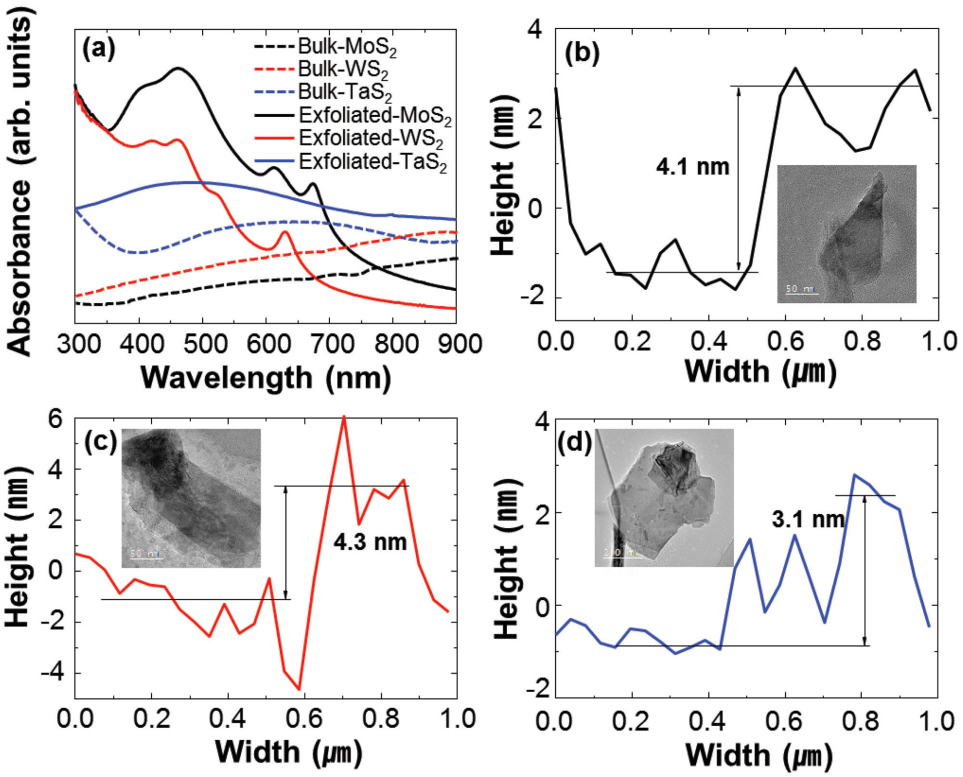

Figure 2. a) UV–vis absorption spectra of TMD nanosheets. The height profiles of b) MoS_2, c) WS_2, and d) TaS_2 nanosheets on SiO2/Si substrates. TEM images of examples of each TMD nanosheet are shown in the insets of (b–d).

increased from 0 to 0.70 and 0.83, respectively, following UVO treatment. The appearances of the Mo^{6+} and W^{6+} peaks and the decreases in the intensities of the Mo^{4+} and W^{4+} peaks indicate that portions of MoS_2 and WS_2 were converted to MoO_x and WO_x, respectively, by UVO treatment. In the case of the O 1s spectra, the O 1s peak was located at 532.3 eV in the MoS_2 spectrum and 531.8 eV in WS_2 spectrum, indicating the presences of adsorbed oxygen on the surfaces of the films. After UVO treatment for 15 min, a new O 1s peak appeared at 531.0 eV in the MoS_2 spectrum and 530.7 eV in the WS_2 spectrum, corresponding to oxygen bonding with Mo^{6+} and W^{6+}, respectively. The Ta 4f peak of the TaS_2 spectrum is composed of two doublets. One of the doublets indicates binding energies of 24.7 and 26.6 eV, corresponding to Ta^{4+} $4f_{7/2}$ and Ta^{4+} $4f_{5/2}$ transitions, respectively. The other doublet peaks, located at 26.9 and 28.8 eV, indicate Ta^{5+} $4f_{7/2}$ and Ta^{5+} $4f_{5/2}$ transitions of Ta_2O_5, which is formed during fabrication. The intensity of the Ta^{5+} portion of the Ta 4f peak increased from 0.24 to 0.47 after UVO treatment, suggesting that Ta_2O_5 was formed. The O 1s peak of the TaS_2 sample was composed of two peaks. The peak located at 531.6 eV indicates bonding between oxygen and Ta^{5+}. The other peak, located at 532.9 eV, is attributed to oxygen adsorbed to the sample surface. The intensity of the O–Ta^{5+} portion of the O 1s spectrum increased from 0.36 to 0.66 after UVO treatment. These results indicate that the TMD nanosheets were partially converted to their oxides during UVO treatment.

Changes in the work functions of the TMD nanosheets following UVO treatments were measured by secondary electron emission spectroscopy, as shown in **Figure 6**a. The onsets of

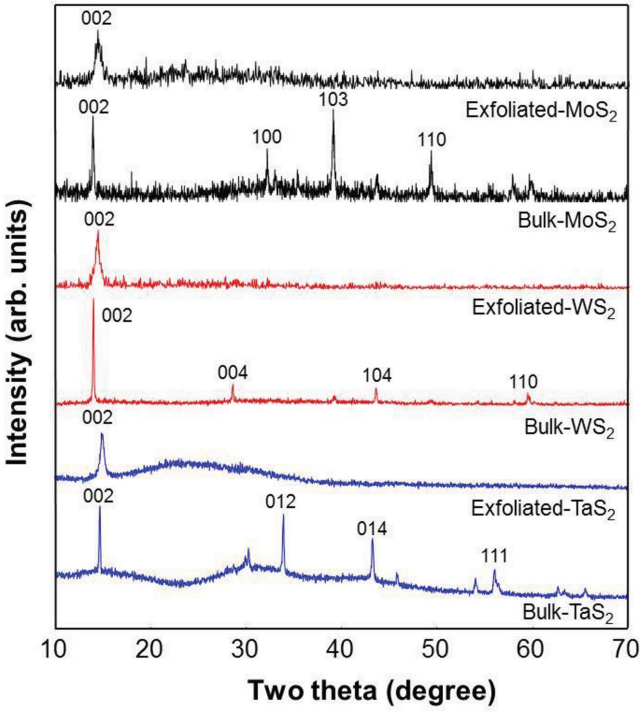

Figure 3. XRD patterns of exfoliated TMDs and bulk TMDs. The bulk materials have various peaks due to the lattice structure of materials. Exfoliated TMDs has only orientation plane of (002), indiating that one layer or few-layers of TMDs nanosheets were successfully made through the exfoliation process.

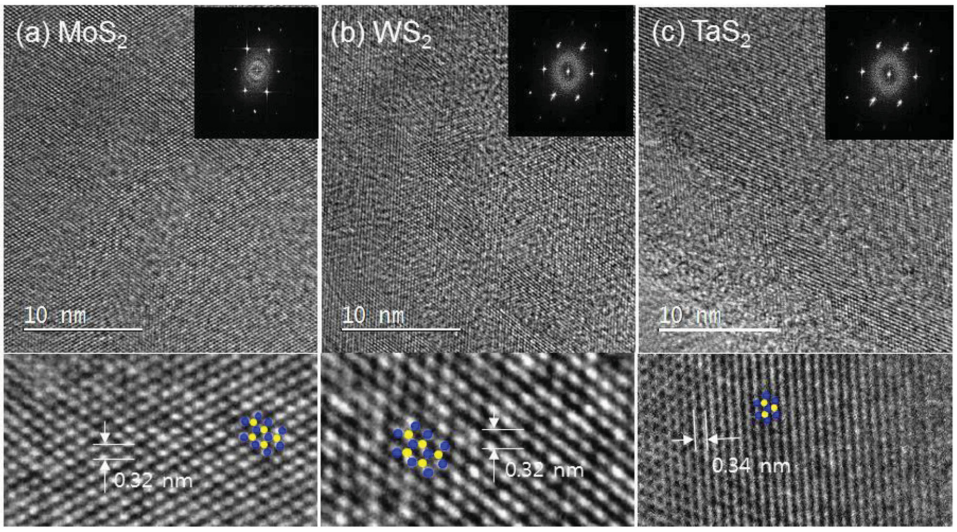

Figure 4. TEM images of a) MoS_2, b) WS_2, and c) TaS_2. SAED patterns of exfoliated TMDs show hexagonal structure. Metal atoms are indicated as yellow color and sulfur atoms are indicated as blue color.

secondary electron emissions were determined by extrapolating the linear backgrounds and straight onsets of the spectra.[31] The work functions of the MoS_2, WS_2, and TaS_2 nanosheets were determined to be 3.9, 4.9, and 4.4 eV, respectively. After UVO treatment, these values increased to 4.9, 5.1, and 4.9 eV for the MoS_2, WS_2, and TaS_2 nanosheets, respectively. It is assumed that UVO treatment introduces oxygen into the lattices of TMD nanosheets, thereby forming partial oxide layers, leading to increases in work functions. Figure 6b shows a band diagram describing OLEDs. The energy levels of each layer were obtained from the literature.[32] According to the band diagram, the hole injection barriers between the TMDs and NPB were reduced from 0.9, 0.6, and 1.1 eV to 0.6, 0.4, and 0.6 eV for MoS_2, WS_2, and TaS_2, respectively, during UVO treatment. This means that the work functions of UVO-treated TMD nanosheets make them appropriate for use as HILs in OLEDs devices.

Current density–voltage and luminance–voltage data are shown in **Figure 7**a,b. The 10 cd m^{-2} turn-on voltages for OLEDs based on MoS_2, WS_2, and TaS_2 HILs were 7.3, 8.8, and 12.8 V, respectively. In contrast, turn-on voltages for OLEDs made with UVO-treated HIL materials were significantly lower, 4.4, 4.35, and 4.3 V for MoS_2, WS_2, and TaS_2, respectively. The maximum luminance efficiencies measured on MoS_2, WS_2, and TaS_2-based devices were 8.71, 5.74, and 9.04 cd A^{-1}, respectively. Following UVO treatment, efficiencies increased, remarkably, to 12.01, 12.44, and 12.66 cd A^{-1} for MoS_2-, WS_2-, and TaS_2-based devices, respectively. This suggests that UVO treatments modulate work functions by lowering hole injection barriers, as shown in Figure 6. The efficiencies of the OLEDs produced using UVO treated HIL materials were slightly lower than that of a PEDOT:PSS-based OLED (13.15 cd A^{-1}). Furthermore, UVO-treated TMD-based devices show much higher maximum power efficiencies (UVO-treated MoS_2 = 3.43 lm W^{-1}, UVO-treated WS_2 = 3.55 lm W^{-1}, UVO-treated TaS_2 = 4.77 lm W^{-1}) than those of untreated TMD-based devices (MoS_2 = 2.17 lm W^{-1}, WS_2 = 0.97 lm W^{-1}, TaS_2 = 2.07 lm W^{-1}). A summary of the device characteristics is given in **Table 1**. These results indicate that UVO treatment of TMD nanosheets modulates their work functions and improves OLED characteristics.

The stabilities of the UVO-treated TMD and PEDOT:PSS-based devices were investigated without encapsulation, in air, using a constant current density of 1 mA cm^{-2}, as shown in **Figure 8**a. In the case of the PEDOT:PSS-based device, most of the active area darkened, as a result of degradation in air, after 72 h, while the dark spots of the other devices were smaller. In particular, the UVO-treated TaS_2-based device was still bright after 120 h. It is reported that electrical resistivity of TaS_2 (10^{-3} Ω cm) is much lower than that of MoS_2 and WS_2 (18 and 0.1 Ω cm).[33–35] Therefore, it is considered that device based on TaS_2 displays the highest stability even though the charge injection barrier is not the smallest. This shows that the stabilities of the UVO-treated TMD-based devices were extended compared to the PEDOT:PSS-based device. After 72 h, voltages were 4.25, 3.35, 3.14, and 3.02 V for PEDOT:PSS, UVO-treated MoS_2-, WS_2-, and TaS_2-based devices, respectively, as shown in Figure 8b. These results indicate that replacing PEDOT:PSS HILs with UVO-treated TMD nanosheet HILs could improve OLED stability because they are nonacidic and chemically stable.

3. Conclusion

TMD nanosheets were prepared, using an exfoliation method, and used as HILs in OLEDs to improve device characteristics. UV–vis spectra indicate that band gaps of approximately 1.70, 1.80, and 1.63 eV were formed in MoS_2, WS_2, and TaS_2 nanosheets, respectively, suggesting that bulk-TMDs are changed to a few layers of TMD nanosheets. The thicknesses and sizes of the TMD nanosheets were measured to be 3.1–4.3 nm and more than 100 nm, respectively. After UVO treatment of the TMD nanosheets, peak intensities increased for Mo^{6+} 3d, W^{6+} 4f, and Ta^{5+} 4f transition metal peaks, and the transition metal-oxide bond peaks in the O 1s spectra

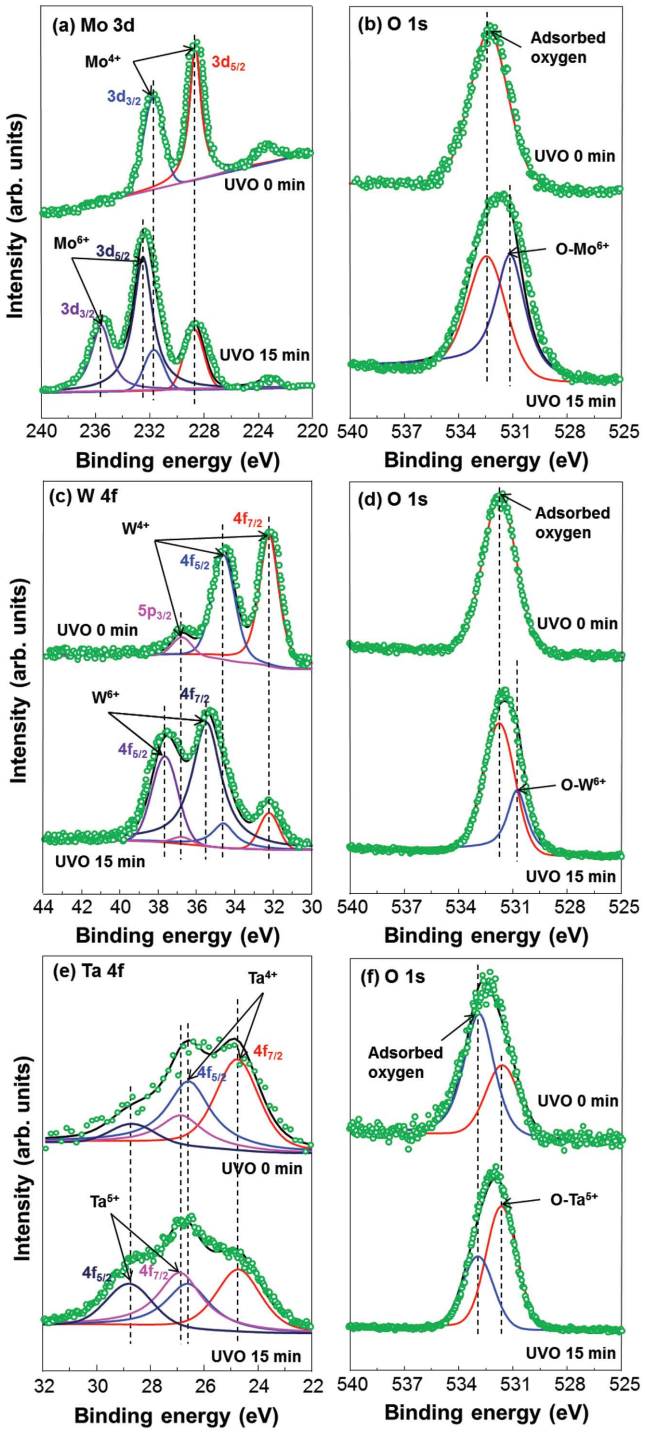

Figure 5. SRPES spectra of a) Mo 3d and b) O 1s peaks in MoS_2 nanosheets, c) W 4f and d) O 1s in WS_2 nanosheets, and e) Ta 4f and f) O 1s peaks in TaS_2 nanosheets. The spectral line shape was simulated using a suitable combination of Gaussian and Lorentzian functions to separate the chemical bonding states. For all multiplets that were fit, the full-width at half-maximum values were fixed accordingly.

indicated that the TMD nanosheets were partially converted into oxides. Therefore, work functions increased from 4.4–4.9 to 4.9–5.1 eV. This finding was confirmed by secondary electron

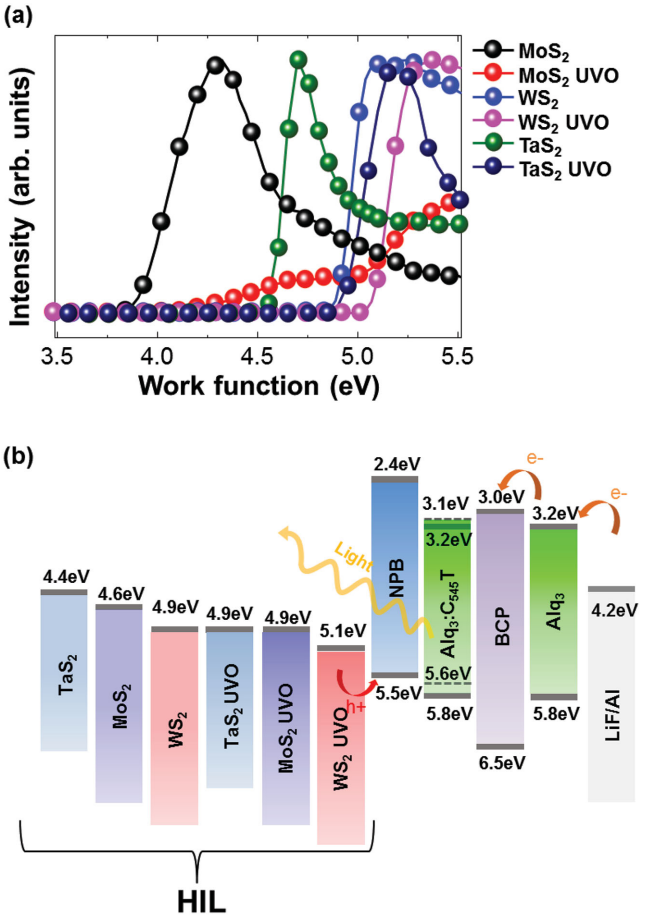

Figure 6. a) The change in onset of secondary electron of TMDs nanosheets before and after UVO treatment. b) Schematic band diagram of OLEDs.

emission spectroscopy. When UVO-treated TMDs were used as HILs in OLEDs, turn-on voltages decreased from 7.3–12.8 to 4.3–4.4 V and luminance efficiencies increased from 5.74–9.04 to 12.01–12.66 cd A^{-1}. Furthermore, it is worth noting that the UVO-treated TMD nanosheet-based OLEDs were more stable than the PEDOT:PSS-based OLED, when not encapsulated and under atmospheric condition. These results show the great potential of liquid-exfoliated TMD nanosheets for us as HILs in OLEDs.

4. Experimental Section

Synthesis: MoS_2, WS_2, and TaS_2 powders and *N*-vinylpyrrolidone (NVP) were purchased from Sigma-Aldrich. An ultrasonicator (SONICS VCX-750, Sonicator Microtip Probes) was used to exfoliate TMD powders. Samples were synthesized by first dispersing 30 mg of TMD powder in 10 mL of NVP and then ultrasonicating the dispersion for 8 h at 400 W. After ultasonication, samples were centrifuged (DAIHAN WiseSpin CF-10) for 10 min at 10 000 rpm. The floating solutions, which contained exfoliated TMDs, were pipetted off and NVP solvent was removed by washing with isopropanol. The final products were dried at 30 °C in a vacuum oven and the obtained TMD nanosheets were redispersed in NVP for further processing.

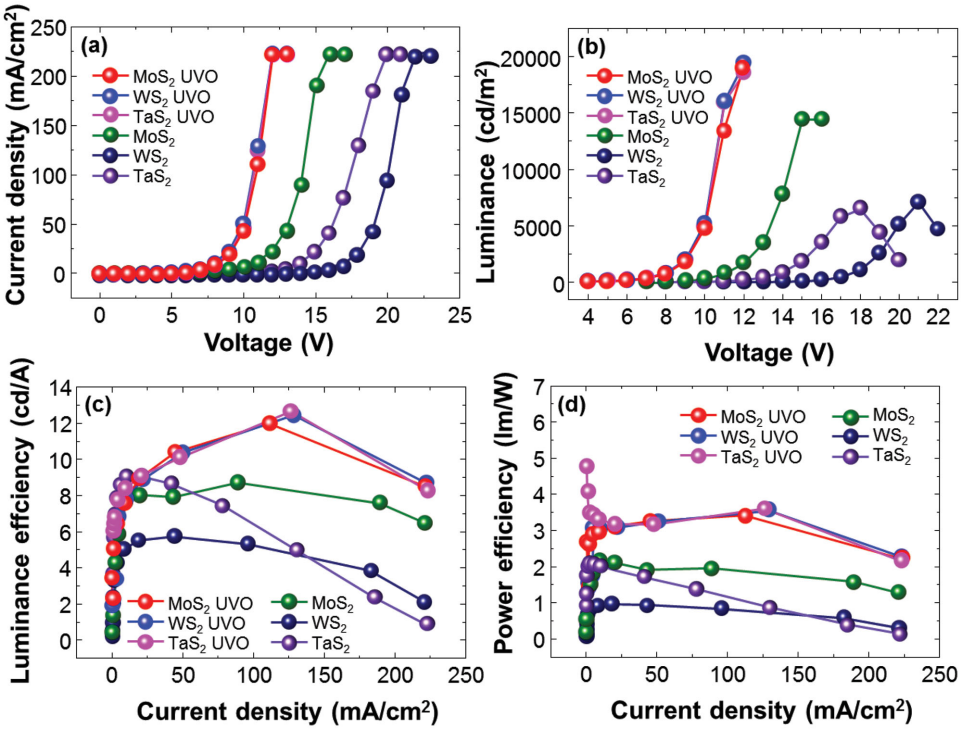

Figure 7. The a) current density–voltage, b) luminance–voltage, c) luminance efficiency–current density, and d) power efficiency–current density characteristics of OLEDs with six different types of OLEDs.

OLEDs Fabrication: Green OLEDs were fabricated on glass substrates coated with ITO. The ITO glasses were cleaned with acetone, isopropyl alcohol, and deionized water, in sequence, then dried and exposed to UVO for 15 min. MoS_2, WS_2, and TaS_2 nanosheets in NVP (1 mg mL^{-1}) were spin-coated at 6000 rpm for 45 s, then dried at 150 °C in air for 15 min. Next, UVO treatment was performed for 15 min. For the sake of comparison, PEDOT:PSS was spin-coated at 4000 rpm for 30 s and annealed at 150 °C in air for 15 min. A 40 nm thick layer of *N*,*N*′-Di(1-naphthyl)-*N*,*N*′-diphenyl-(1,1′-biphenyl)-4,4′-diamine (NPB) was used as a hole transport layer. A 30 nm thick layer of tris-(8-hydroxyquinoline) aluminum (Alq_3) was used as a host layer. The emitting layer was comprised of 2,3,6,7-tetrahydro-1,1,7,7,-tetramethyl-1H, 5H, doped with 5% 11H-10-(2-benzothiazolyl)quinolizino[9,9a,1gh]coumarin (C545T). A 5 nm thick bathocuproine (BCP) was employed as the hole-blocking layer. Finally, a 25 nm thick layer of Alq_3 was used as the electron transport layer. All layers were deposited using a vacuum of about 2×10^{-6} Torr and a deposition rate of 1 Å s^{-1}. Finally, a 1 nm thick layer of LiF and a 100 nm thick layer of Al were thermally deposited. The OLED device structure is illustrated in Figure 1.

Characterization: A Keithley 2622A source meter was used in conjunction with a MINOLTA CS100A luminance meter to measure the current–voltage–luminance characteristics and Commission Internationale de l'Eclairage (CIE) chromaticity coordinates of the OLED devices produced. UV–vis absorption spectra (V-670 UV–vis spectrophotometer) were measured to confirm the optical properties of the TMDs. Contact mode AFM (XE-100/PSIA) was used to determine the thicknesses of the exfoliated TMD nanosheets. XRD pattern (D8-Advance/Bruker-AXS) and TEM (JEOL-2100F, Japan) images were obtained to measure the structure and sizes of the TMD nanosheets. SRPES experiments were also performed in an ultrahigh-vacuum chamber (base pressure of $\approx 10^{-10}$ Torr) at the 4D beam line of the Pohang Acceleration Laboratory. The onset of photoemission, corresponding to the vacuum level at the surface of a TMD nanosheet, was measured using an incident photon energy of 90 eV and a negatively

Table 1. The summary of OLEDs characteristics.

	Turn-on voltage [V][a)]	Luminance^{max} [cd m^{-2}]	Luminance efficiency^{max} [cd A^{-1}]	Power efficiency^{max} [lm W^{-1}]	CIE1931 coordinates [*x*, *y*]
PEDOT:PSS	3.95	21 400	13.12	6.22	(0.30, 0.66)
MoS_2 UVO	4.4	18 900	12.01	3.43	(0.31, 0.64)
WS_2 UVO	4.35	19 300	12.44	3.55	(0.30, 0.65)
TaS_2 UVO	4.3	18 400	12.66	4.77	(0.30, 0.65)
MoS_2	7.3	14 400	8.71	2.17	(0.30, 0.65)
WS_2	8.8	7050	5.74	0.97	(0.30, 0.65)
TaS_2	12.8	6840	9.04	2.07	(0.30, 0.65)

[a)]Turn-on voltages at 10 cd m^{-2}.

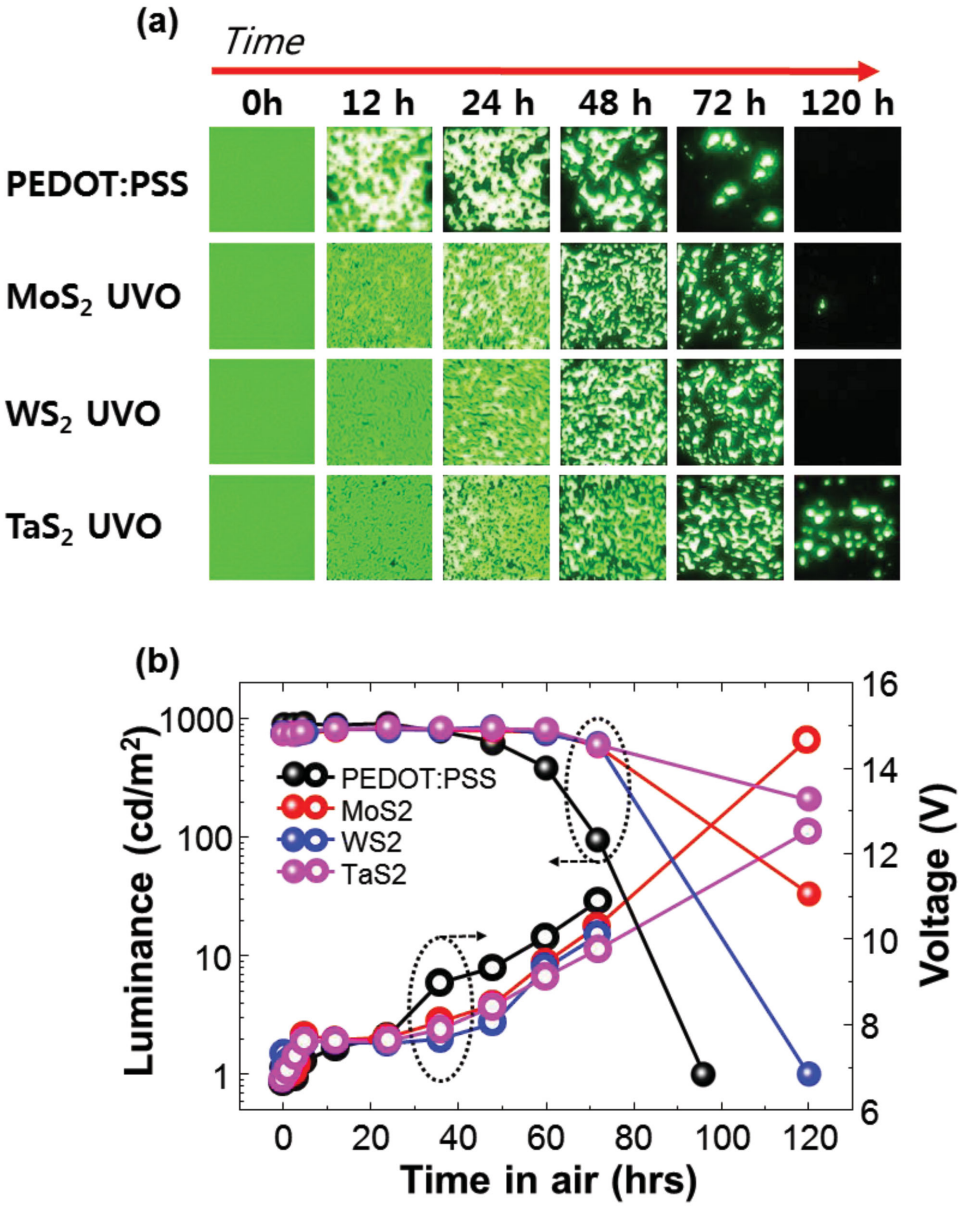

Figure 8. Stability of four types of OLEDs measured under air without encapsulation. a) The actual photographs and b) luminance–voltages of devices according to the time kept in air.

biased sample. Results were corrected for charging effects using a Au internal reference.

Received: April 3, 2015
Revised: May 19, 2015
Published online: June 15, 2015

Supporting Information

Supporting Information is available from the Wiley Online Library or from the author.

Acknowledgements

C.K. and T.P.N. contributed equally to this work. This work was supported by Samsung Research Funding Center of Samsung Electronics under Project Number SRFC-MA1402-14.

[1] H. Sasabe, J. Kido, *J. Mater. Chem. C.* **2013**, *1*, 1699.
[2] J. Wang, F. Zhang, Z. Zhang, W. Tang, A. Tang, H. Peng, Z. Xu, F. Teng, T. Wang, *J. Photochem. Photobiol. C: Photochem. Rev.* **2013**, *17*, 69.
[3] B. Geffroy, P. Roy, C. Prat, *Polym. Int.* **2006**, *55*, 572.
[4] L. Xiao, Z. Chen, B. Qu, J. Luo, S. Kong, Q. Gong, J. Kido, *Adv. Mater.* **2011**, *23*, 926.
[5] S. T. Lee, Y. M. Wang, X. T. Hou, C. W. Tang, *Appl. Phys. Lett.* **1999**, *74*, 670.

[6] Z. Sun, B. Ding, B. Wu, Y. You, X. Ding, X. Hou, *J. Phys. Chem. C.* **2012**, *116*, 2543.
[7] Y.-F. Zhou, Y.-B. Yuan, L-F. Cao, J. Zhang, H.-Q. Pang, J.-R. Lian, X. Zhou, *J. Lumin.* **2007**, *122*, 602.
[8] M. P. de Jong, L. J. van IJzendoorn, M. J. A. de Voigt, *Appl. Phys. Lett.* **2000**, *77*, 2255.
[9] Q. H. Wang, K. Kalantar-Zadeh, A. Kis, J. N. Coleman, M. S. Strano, *Nat. Nanotechnol.* **2012**, *7*, 699.
[10] X. Huang, Z. Zeng, H. Zhang, *Chem. Soc. Rev.* **2013**, *42*, 1934.
[11] M. Chhowalla, H. S. Shin, H. Eda, L.-J. Li, K. P. Loh, H. Zhang, *Nat. Chem.* **2013**, *5*, 263.
[12] R. Lv, J. A. Robinson, R. E. Schaak, D. Sun, Y. Sun, T. E. Mallouk, M. Terrones, *Acc. Chem. Res.* **2015**, *48*, 56.
[13] Q. V. Le, T. P. Nguyen, K. C. Choi, Y.-H. Cho, Y. J. Hong, S. Y. Kim, *Phys. Chem. Chem. Phys.* **2014**, *16*, 25468.
[14] D. Jariwala, V. K. Sangwan, L. J. Lauhon, T. J. Marks, M. C. Hersam, *ACS Nano* **2014**, *8*, 1102.
[15] H. Fang, S. Chuang, T. C. Chang, K. Takei, T. Takahashi, A. Javey, *Nano Lett.* **2012**, *12*, 3788.
[16] Q. V. Le, T. P. Nguyen, S. Y. Kim, *Phys. Status Solidi RRL* **2014**, *8*, 1.
[17] R. S. Sundaram, M. Engel, A. Lombardo, R. Krupke, A. C. Ferrari, P. Avouris, M. Steiner, *Nano Lett.* **2013**, *13*, 1416.
[18] L. Britnell, R. M. Ribeiro, A. Eckmann, R. Jalil, B. D. Belle, A. Mishchenko, Y.-J. Kim, R. V. Gorbachev, T. Georgiou, S. V. Morozov, A. N. Grigorenko, A. K. Geim, C. Casiraghi, A. H. Castro Neto, K. S. Novoselov, *Science* **2013**, *340*, 1311.
[19] G. Cunninghan, M. Lotya, C. S. Cucinotta, S. Sanvito, S. D. Bergin, R. Menzel, M. S. P. Shaffer, J. N. Coleman, *ACS Nano* **2012**, *6*, 3468.
[20] Y.-H. Lee, X.-Q. Zhang, W. Zhang, M.-T. Chang, C.-T. Lin, K.-D. Chang, Y.-C. Yu, J. T. -W. Wang, C.-S. Chang, L.-J. Li, T.-W. Lin, *Adv. Mater.* **2012**, *24*, 2320.
[21] J. N. Coleman, M. Lotya, A. O'neill, S. D. Bergin, P. J. King, U. Khan, K. Young, A. Gaucher, S. De, R. J. Smith, I. V. Shvets, S. K. Arora, G. Stanton, H.-Y. Kim, K. Lee, G. T. Kin, G. S. Duesberg, T. Hallam, J. J. Boland, J. J. Wang, J. F. Donegan, J. C. Grunlan, G. Moriaty, A. Shmeliov, R. J. Nicholls, J. M. Perkins, E. M. Griveson, K. Theuwissien, D. W. McComb, P. D. Nellist, V. Nicolosi, *Science* **2011**, *331*, 568.
[22] H. Li, Z. Yin, Q. He, H. Li, X. Huang, G. Lu, D. W. H. Fam, A. Y. Tok, Q. Zhang, H. Zhang, *Small* **2012**, *8*, 63.
[23] Z. Zeng, Z. Yin, X. Huang, H. Li, Q. He, G. Lu, F. Boey, H. Zhang, *Angew. Chem. Int. Ed.* **2011**, *50*, 11093.
[24] H. Li, J. Wu, Z. Yin, H. Zhang, *Acc. Chem. Res.* **2014**, *47*, 1067.
[25] Z. Yin, H. Li, H. Li, L. Jiang, Y. Shi, Y. Sun, G. Lu, Q. Zhang, X. Chen, H. Zhang, *ACS Nano* **2012**, *6*, 74.
[26] Z. Yin, X. Zhang, Y. Cai, J. Chen, J. I. Wong, Y.-Y. Tay, J. Chai, J. Wu, Z. Zeng, B. Zheng, H. Y. Yang, H. Zhang, *Angew. Chem. Int. Ed.* **2014**, *53*, 12560.
[27] X. Gu, W. Cui, T. Song, C. Liu, X. Shi, S. Wang, B. Sun, *ChemSusChem.* **2014**, *7*, 416.
[28] X. Gu, W. Cui, H. Li, Z. Wu, Z. Zeng, S.-T. Lee, H. Zhang, B. Sun, *Adv. Energy Mater.* **2013**, *3*, 1262.
[29] V. Stengl, J. Henych, *Nanoscale* **2013**, *5*, 3387.
[30] Y. Yu, C. Li, Y. Liu, L. Su, Y. Zhang, L. Cao, *Sci. Rep.* **2013**, *3*, 1866.
[31] K. C. Kwon, J. Ham, S. Kim, J.-L. Lee, S. Y. Kim, *Sci. Rep.* **2014**, *4*, 4830.
[32] K. C. Kwon, S. Kim, C. Kim, J.-L. Lee, S. Y. Kim, *Org. Electron.* **2013**, *15*, 3154.
[33] F. J. Di Salvo, J. E. Graebner, *Solid State Commun.* **1977**, *23*, 825.
[34] A. J. Grant, T. M. Griffiths, G. D. Pitt, A. D. Yoffe, *J. Phys. C: Solid State Phys.* **1975**, *8*, L17.
[35] T. J. Wieting, *J. Phys. Chem. Solids* **1970**, *31*, 2148.